

An *in vivo* Comparison of Principal and Polar Strains in Carotid Atherosclerotic Plaques

Yuanyuan Wang¹, Zhi Liu¹, Qiong He¹, Xuejiao Wang², Zhen Yang², Changming Wang^{3*}, Ligang Cui^{2*}, and Jianwen Luo^{1*}

¹Department of Biomedical Engineering, School of Medicine, Tsinghua University, Beijing, China

²Department of Sonography, Peking University Third Hospital, Beijing, China

³Department of Vascular Surgery, Peking University Third Hospital, Beijing, China

E-mail: wcmwy@163.com, ligangcui@pku.edu.cn and luo_jianwen@tsinghua.edu.cn

Abstract—Rupture of carotid atherosclerotic plaques is one of the major causes of cerebrovascular events. Polar strains in the cross-sectional carotid elastography have been demonstrated to identify vulnerable plaques. However, the vessel center used to calculate the polar strains is difficult to estimate precisely in carotid arteries with plaques. To solve this problem, principal strains which can be measured without identification of the vessel center are proved consistent with polar strains in healthy volunteers. In this study, we compared the performance of principal and polar strains in assessing the elasticity of carotid atherosclerotic plaques. Ultrasound radiofrequency data were acquired from 13 carotid plaques of 9 patients, in the transversal imaging views. The inter-frame axial and lateral strains were obtained using an affine model-based spatial angular compounding method, which were further transformed into the polar (radial and circumferential) and principal (minor and major) strains. The maximum, mean, median, standard deviation (SD) and 99th percentile were calculated from the absolute value of each strain for comparison. Statistically significant correlations were found between the maximum, mean, median, SD and 99th percentile calculated from minor principal strain and radial polar strain, as well as between the indices from major principal strain and circumferential polar strain. These findings demonstrate significant correlations between polar and principal strains, and principal strains may be useful indices for assessing the vulnerability of carotid atherosclerotic plaques.

Keywords—carotid atherosclerotic plaques, polar strains, principal strains.

I. INTRODUCTION

Rupture of carotid atherosclerotic plaques is one of the major causes of stroke. Identification of vulnerable plaques is essential for prevention of ischemic events and decision-making in clinical treatment. It is widely acknowledged that plaques with calcification, thick fibrous cap and intact surface are more likely to be stable, while those with a large lipid-rich necrotic core under a thin fibrous cap, intraplaque hemorrhage, inflammation and neovasculature are more susceptible to be vulnerable [1]. Histological study of plaques have found that different compositions have different mechanical properties [2]. On this premise, taking the advantage of high temporal resolution, non-invasive carotid elastography has been extensively studied for assessing the rupture risk of the atherosclerosis plaques.

Carotid elastography assesses the elasticity of carotid artery and plaque based on the principle that stiffer tissues have smaller deformation than softer tissues when undergoing an external force. Local tissue displacement between the pre- and post-deformation ultrasound images can be estimated based on various motion estimation methods (e.g., normalized cross-correlation [3], sum of squared differences [4], nonrigid image registration [5], and optical flow [6]). Tissue strains can be further obtained by taking spatial derivation of the displacements.

The longitudinal view of the carotid artery is commonly used for assessing the plaque stiffness. Under this view, the radial and longitudinal strains are typically estimated in Cartesian coordinates and the radial strain corresponds to the axial strain assuming that the ultrasound beams are aligned with the radial direction of the artery [7]. Simulations, phantom, *in vitro* and *in vivo* experiments have demonstrated the feasibility of longitudinal carotid elastography [8-10]. Validated by the magnetic resonance imaging or pathological examination, many measurement indices calculated from the longitudinal strains have been reported to differentiate the vulnerable plaques from the stable ones, demonstrating the promise for assessing the plaque rupture risk [11-14].

However, longitudinal scanning cannot detect the plaques on the lateral wall of the carotid artery and reflect mechanical properties of the whole plaque. Thus transverse scanning is required. The plaque motion in the transverse view is in the radial and circumferential directions and thus a polar coordinate system is established. The polar (radial and circumferential) strains are calculated by projecting the lateral and axial strains from Cartesian coordinates into polar coordinates. Nevertheless, poor estimation accuracy of lateral strains can deteriorate the estimation of polar strains [15]. To solve the problem, spatial angular compounding (SAC) was proposed to improve the performance of lateral strain estimation and was applied to carotid elastography in the transverse scanning [16-20].

Nevertheless, the lumen center needs to be selected precisely when estimating the polar strains, which is difficult to achieve in the carotid arteries with plaques. Therefore, the principal strains which are independent of the lumen center have attracted increasing research interests recently. The principal strains were first used in myocardial elastography to remove the center-of-heart dependence of strain calculation in

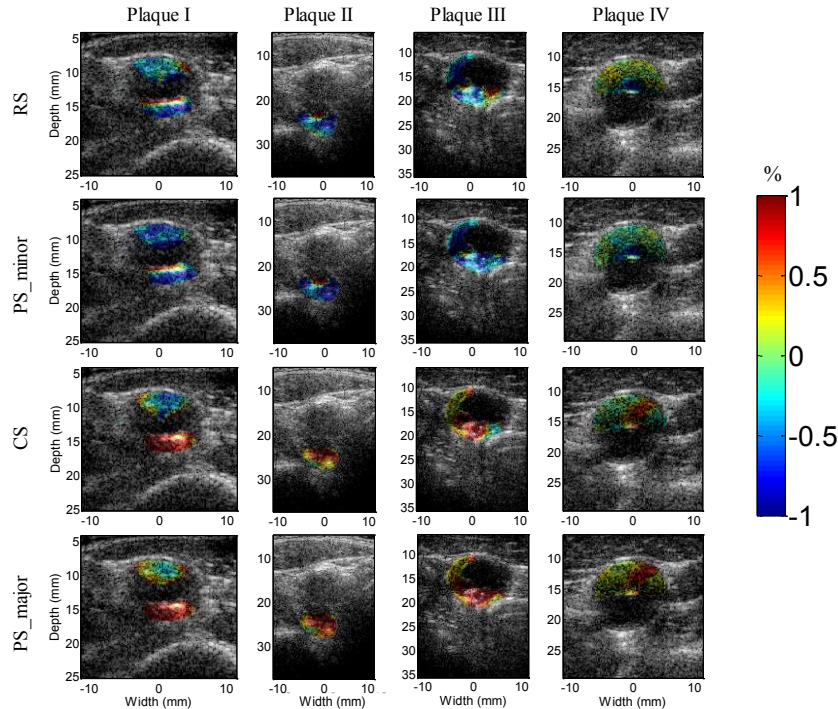


Fig. 1. Different strain images in the maximum deformation obtained from 4 plaques.

order to better assess myocardial ischemia and myocardial abnormalities [21]. In the field of carotid elastography, Poree *et al.* verified the feasibility of principal strains in evaluating blood vessel elasticity [22]. Besides, Nayak *et al.* explored the differences between polar and principal strains using simulations and *in vivo* experiments on normal human carotid artery, and found no significant difference between radial strain (RS) and minor principal strain (PS_minor), as well as between circumferential strain (CS) and major principal strain (PS_major) [23]. But there are no studies yet to compare the performances of these two strains on carotid plaques, which is crucial for plaque elasticity assessment.

Therefore, the objective of this study was to compare the performance of polar and principal strains in carotid atherosclerotic plaques.

II. METHODS

A. Data acquisition

13 carotid atherosclerotic plaques from 9 patients were scanned using Verasonics Vantage system and L12-5 linear-array probe with the center frequency of 6.25 MHz. Plane waves with 5 steering angles (-15° , -5° , 0° , 5° , 15°) were transmitted at a PRF of 5000 Hz. Ultrasound radiofrequency (RF) channel data were acquired from the transverse imaging views at a sampling frequency of 31.25 MHz. The acquisition time for each plaque was 3 s. After acquiring the channel data, the delay-and-sum (DAS) algorithm with a Hanning apodization and an f-number of 1.5 was used to obtain the post-beamformed RF data.

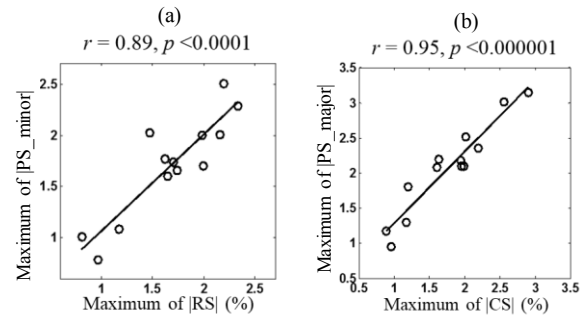


Fig. 2. (a) Relationship between the maximum values from PS_minor and RS. (b) Relationship between the maximum values from PS_major and CS.

B. Strain estimation

An affine model-based spatial angular compounding method proposed in [24] was used to estimate the inter-frame lateral and axial displacements from the post-beamformed RF data of the carotid plaques. The plaques were segmented manually on the B-mode images to obtain the inter-frame displacements of the plaques.

A Cartesian coordinate system using the probe center as the coordinate origin was built. The normal strains (i.e., lateral and axial strains) and the shear strains (i.e., lateral shear and axial shear strain) were estimated under this coordinate by taking spatial gradients of the displacements using a Savitzky-Golay (SG) filter. The polar strains (RS and CS) were further estimated by projecting the normal and shear strains in the Cartesian coordinates into the polar coordinates using the lumen center as the coordinate origin [25]. In this study, the center of the carotid artery was manually selected according to the corresponding color flow image. In contrast, the principal

Table I. Pearson correlation (r) between PS_minor and RS, PS_major and CS, in terms of different measurement indices.

| | Maximum | | Mean | | Median | | SD | | 99 th percentile | |
|----------------|-----------------|-----------------|-----------------|-----------------|-----------------|-----------------|-----------------|-----------------|-----------------------------|-----------------|
| | PS_minor vs. RS | PS_major vs. CS | PS_minor vs. RS | PS_major vs. CS |
| r | 0.89 | 0.95 | 0.89 | 0.94 | 0.86 | 0.94 | 0.95 | 0.87 | 0.87 | 0.93 |
| 95% CI | 0.67-0.97 | 0.84-0.99 | 0.68-0.97 | 0.80-0.98 | 0.59-0.96 | 0.79-0.98 | 0.83-0.98 | 0.62-0.96 | 0.61-0.96 | 0.76-0.98 |
| P value | <0.0001 | <0.000001 | <0.0001 | <0.00001 | <0.001 | <0.00001 | <0.00001 | <0.0001 | <0.001 | <0.00001 |

strains, which are independent of the lumen center, were calculated as described in [23].

C. Data analysis

After obtaining the strains, the frame with the maximum absolute value of each strain, i.e., the frame with the maximum deformation of the plaques, was picked out according to the strain-time curve from a selected point. The inter-frame strains were overlaid on the corresponding B-mode images.

The maximum, mean, median, standard deviation (SD) and 99th percentile were calculated from the absolute value of each maximum strain as the indices for plaque elasticity assessment. These indices derived from PS_minor and PS_major were correlated with those from RS and CS, respectively, using Pearson correlation analysis.

III. RESULTS

The inter-frame RS, PS_minor, CS and PS_major distributions at the frame with the maximum deformation during one cardiac cycle from 4 plaques are illustrated in Fig. 1. As shown, for each plaque, the distribution and magnitude of RS appear close to those of PS_minor. Similar phenomena can also be observed between CS and PS_major. Besides, different strain distributions and magnitudes are found among different plaques, which may be related to varied conditions of different plaques.

Figure 2 shows the Pearson correlation analysis results of the maximum strains calculated from 13 plaques. It can be observed that statistically significant correlations are found between the maximums calculated from PS_minor and RS ($r = 0.89$, $p < 0.0001$), as well as between the maximums obtained from PS_major and CS ($r = 0.95$, $p < 0.000001$).

Table I summarizes the results of Pearson correlation analysis between different measurement indices calculated from PS_minor and RS, as well as from PS_major and CS, respectively. As shown, the mean, median, SD and 99th percentile calculated from PS_minor and RS are significantly correlated. Such correlations can also be found between PS_major and CS. Specifically, the SDs calculated from PS_minor and RS have the highest correlation among all the indices ($r = 0.95$, 95% confidence interval: $0.83 \sim 0.98$, $p < 0.00001$), while the maximums calculated from PS_major and CS show the highest correlation ($r = 0.95$, 95% confidence interval: $0.84 \sim 0.99$, $p < 0.000001$).

IV. DISCUSSION

In this study, we compared the performance of polar and principal strains in carotid atherosclerotic plaques. The strain images (Fig. 1) showed that the distribution and magnitude of inter-frame RS were close to those of PS_minor. Similarly, the distribution and magnitude of CS were close to those of PS_major. Besides, statistically significant correlations were found between all the measurement indices (the maximum, mean, median, SD and 99th percentile) calculated from RS and PS_minor, as well as between those calculated from CS and PS_major (Fig. 2 and Table I).

Many studies have reported that RS and CS perform well in simulations, vessel phantom and *in vivo* carotid artery experiments based on the premise that the vessel center is selected precisely [17, 20, 25]. In the simulations, vessel phantom and healthy carotid artery experiments, the lumen center can be easily identified because the interface between the vascular wall and liquid (blood or distilled water) inside the lumen is clear. However, in the carotid artery with plaques, because of the complex echo intensities of the plaques, it is difficult to identify the lumen center. Color flow images are usually needed to assist the identification. To solve the problem, principal strains which are independent of the lumen center are estimated in carotid elastography. The performance of polar strains and principal strains in carotid elastography has been compared in simulations and phantom experiments, as well as in the carotid arteries from healthy volunteers [22, 23]. Good consistency was found between RS and PS_minor, as well as between CS and PS_major in these experiments. In this study, we compared the performance of polar and principal strains in carotid atherosclerotic plaques and found significant correlations between these two strains. Considering that the estimation of principal strains do not rely on the selection of lumen centers, principal strains may be more potential indices for assessing plaque vulnerability.

In the future, the sample size will be enlarged. Pathological examination will be conducted on the plaques obtained through carotid endarterectomy, as a “golden standard” to assess plaque vulnerability. The performance of polar and principal strains in assessing the plaque vulnerability will be further evaluated and compared.

V. CONCLUSION

In this study, a comparison of principal and polar strains was conducted on 13 carotid atherosclerotic plaques from 9 patients. Significant correlations were found between the measurement indices calculated from the minor principal strain and radial strain, as well as between those from the major principal strain and circumferential strain. Principal strains can be measured without identification of the lumen center and may be useful indices for assessing the vulnerability of carotid atherosclerotic plaques.

ACKNOWLEDGMENT

This study was supported in part by the National Natural Science Foundation of China (81561168023, 61871251 and 61801261) and the China Postdoctoral Science Foundation (2017M620802).

REFERENCES

- [1] E. Falk, P. K. Shah, and V. Fuster, "Coronary plaque disruption," *Circulation*, vol. 92, pp. 657-671, 1995.
- [2] R. T. Lee, S. G. Richardson, H. M. Loree, A. J. Grodzinsky, S. A. Gharib, F. J. Schoen, and N. Pandian, "Prediction of mechanical properties of human atherosclerotic tissue by high-frequency intravascular ultrasound imaging. An in vitro study," *Arteriosclerosis and Thrombosis: A Journal of Vascular Biology*, vol. 12, pp. 1-5, 1992.
- [3] J. Luo and E. E. Konofagou, "A fast normalized cross-correlation calculation method for motion estimation," *IEEE Transactions on Ultrasonics, Ferroelectrics, and Frequency Control*, vol. 57, pp. 1347-1357, 2010.
- [4] L. N. Bohs and G. E. Trahey, "A novel method for angle independent ultrasonic imaging of blood flow and tissue motion," *IEEE Transactions on Biomedical Engineering*, vol. 38, pp. 280-286, 1991.
- [5] M. J. Ledesma-Carbayo, J. Kybic, M. Desco, A. Santos, M. Suhling, P. Hunziker, and M. Unser, "Spatio-temporal nonrigid registration for ultrasound cardiac motion estimation," *IEEE Transactions on Medical Imaging*, vol. 24, pp. 1113-1126, 2005.
- [6] B. Thomas and M. Jitendra, "Large displacement optical flow: descriptor matching in variational motion estimation," *IEEE Transactions on Pattern Analysis & Machine Intelligence*, vol. 33, pp. 500-513, 2011.
- [7] R. L. Maurice and N. Dahdah, "Characterization of aortic remodeling following Kawasaki disease: Toward a fully developed automatic biparametric model," *Medical Physics*, vol. 39, pp. 6104-6110, 2012.
- [8] O. Bonnefous, M. Montaudon, J. C. Sananes, and E. Denis, "Noninvasive echographic techniques for arterial wall characterization," in *Ultrasonics Symposium*, 1996.
- [9] H. Hideyuki and K. Hiroshi, "Simultaneous imaging of artery-wall strain and blood flow by high frame rate acquisition of RF signals," *IEEE Transactions on Ultrasonics, Ferroelectrics, and Frequency Control*, vol. 55, p. 2626, 2008.
- [10] K. Hiroshi, H. Hideyuki, I. Masataka, T. Fumiaki, and K. Yoshiro, "Elasticity imaging of atheroma with transcutaneous ultrasound: preliminary study," *Circulation*, vol. 107, pp. 3018-3021, 2003.
- [11] C. Huang, Q. He, M. Huang, L. Huang, X. Zhao, C. Yuan, and J. Luo, "Non-invasive identification of vulnerable atherosclerotic plaques using texture analysis in ultrasound carotid elastography: An in vivo feasibility study validated by magnetic resonance imaging," *Ultrasound in Medicine & Biology*, vol. 43, pp. 817-830, 2017.
- [12] C. Naim, G. Cloutier, E. Mercure, F. Destremes, Z. Qin, W. El-Abyad, S. Lanthier, M. -F. Giroux, and G. Soulez, "Characterisation of carotid plaques with ultrasound elastography: feasibility and correlation with high-resolution magnetic resonance imaging," *European Radiology*, vol. 23, pp. 2030-2041, 2013.
- [13] M.-H. Roy Cardinal, M. H. Heusinkveld, Z. Qin, R. G. Lopata, C. Naim, G. Soulez, and G. Cloutier, "Carotid artery plaque vulnerability assessment using noninvasive ultrasound elastography: Validation with MRI," *American Journal of Roentgenology*, vol. 209, pp. 142-151, 2017.
- [14] Z. Wang, N. Liu, L. Zhang, X. Li, X. Han, Y. Peng, M. Dang, L. Sun, and J. Tian, "Real-time elastography visualization and histopathological characterization of rabbit atherosclerotic carotid arteries," *Ultrasound in Medicine & Biology*, vol. 42, pp. 176-184, 2016.
- [15] H. Ribbers, R. G. P. Lopata, S. Holewijn, G. Pasterkamp, J. D. Blankensteijn, and C. L. D. Korte, "Noninvasive two-dimensional strain imaging of arteries: Validation in phantoms and preliminary experience in carotid arteries in vivo," *Ultrasound in Medicine & Biology*, vol. 33, pp. 530-540, 2007.
- [16] M. Rao, Q. Chen, H. Shi, and T. Varghese, "Spatial-angular compounding for elastography using beam steering on linear array transducers," *Medical Physics*, vol. 33, pp. 618-626, 2006.
- [17] H. H. Hansen, R. G. Lopata, and C. L. de Korte, "Noninvasive carotid strain imaging using angular compounding at large beam steered angles: validation in vessel phantoms," *IEEE Transactions on Medical Imaging*, vol. 28, pp. 872-880, 2009.
- [18] Q. He, L. Tong, L. Huang, J. Liu, Y. Chen, and J. Luo, "Performance optimization of lateral displacement estimation with spatial angular compounding," *Ultrasonics*, vol. 73, pp. 9-21, 2017.
- [19] H. H. G. Hansen, G. J. D. Borst, M. L. Bots, F. L. Moll, G. Pasterkamp, and C. L. D. Korte, "Validation of noninvasive in vivo compound ultrasound strain imaging using histologic plaque vulnerability features," *Stroke*, vol. 47, pp. 2770-2775, 2016.
- [20] H. Hansen, A. Saris, N. Vaka, M. Nillesen, and C. De Korte, "Ultrafast vascular strain compounding using plane wave transmission," *Journal of Biomechanics*, vol. 47, pp. 815-823, 2014.
- [21] I. K. Zervantonakis, S. D. Fung-Kee-Fung, L. W-N, and E. E. Konofagou, "A novel, view-independent method for strain mapping in myocardial elastography: eliminating angle and centroid dependence," *Physics in Medicine & Biology*, vol. 52, pp. 4063-80, 2007.
- [22] J. Poree, D. Garcia, B. Chayer, J. Ohayon, and G. Cloutier, "Noninvasive vascular elastography with plane strain incompressibility assumption using ultrafast coherent compound plane wave imaging," *IEEE Transactions on Medical Imaging*, vol. 34, pp. 2618-2631, 2015.
- [23] R. Nayak, S. Huntzicker, J. Ohayon, N. Carson, V. Dogra, G. Schifitto, and M. M. Doyley, "Principal strain vascular elastography: Simulation and preliminary clinical evaluation," *Ultrasound in Medicine & Biology*, vol. 43, pp. 682-699, 2017.
- [24] Z. Liu, Q. He, and J. Luo, "Spatial angular compounding with affine model based optical flow for improvement of motion estimation," *IEEE Transactions on Ultrasonics, Ferroelectrics, and Frequency control*, vol. 66, pp. 701-716, 2019.
- [25] S. Korukonda and M. M. Doyley, "Visualizing the radial and circumferential strain distribution within vessel phantoms using synthetic-aperture ultrasound elastography," *IEEE Transactions on Ultrasonics, Ferroelectrics, and Frequency control*, vol. 59, pp. 1639-1653, 2012.